Asian Journal of Basic Science & Research
Volume 7, Issue 2, Pages 59-77, April-June 2025

Collagen hydrogel scaffolds with *Hibiscus*-infused silica nanoparticles: A bioactive platform for metabolic stimulation

Alondra G. Álcala-Herrera[1], Martín Caldera-Villalobos[1], María I. León-Campos[1], Lesly Katleya Usme-Duque[1], Tirso E. Flores-Guía[1], Lucía F. Cano-Salazar[1], Denis A. Cabrera-Munguia[1], Miguel A. Medina-Morales[2] & Jesús A. Claudio-Rizo[1*]

[1]*Department of Advanced Materials, Faculty of Chemical Sciences, Autonomous University of Coahuila, Blvd. Venustiano Carranza S/N, República, 25280 Saltillo, Coahuila, México.* [2]*Department of Environmental Biotechnology, Faculty of Chemical Sciences, Autonomous University of Coahuila, Blvd. Venustiano Carranza S/N, República, 25280 Saltillo, Coahuila, México. Email: jclaudio@uadec.edu.mx**

DOI: http://doi.org/10.38177/AJBSR.2025.7207

Article Received: 05 April 2025 *Article Accepted: 09 June 2025* *Article Published: 16 June 2025*

ABSTRACT

In this study, bioactive scaffolds based on type I collagen hydrogels were developed by encapsulating silica nanoparticles (SiNPs) loaded with varying concentrations of *Hibiscus sabdariffa* extract (NpsSHS) (1-3 wt.%). The resulting hybrid materials exhibited semi-crystalline or amorphous structures, with loss of crystallinity corresponding to increased *Hibiscus* content on the scaffold surface. Microstructural analysis revealed that the plant-extract-loaded SiNPs became embedded within the fibrillar collagen matrix, generating an interconnected porous topology favorable for cellular interaction. Higher NpsSHS loading led to reduced swelling capacity—while still achieving superabsorbent behavior (>1200%)—and significantly enhanced the crosslinking degree (up to 68%) and thermal degradation stability of the hydrogels. These effects are attributed to short-range interactions between bioactive phytochemicals in the extract (such as polyphenols, organic acids, and anthocyanins) and the amino and carboxylate groups of collagen. *In vitro* assays showed a significant metabolic activation in various cell types, including immune cells (monocytes), soft tissue-forming cells (fibroblasts), hard tissue-forming cells (bone marrow-derived osteogenic cells), and colon cancer cells. The metabolic stimulation was more pronounced in scaffolds containing higher *Hibiscus* concentrations (up 3 wt.%), indicating the potential of this platform to broadly enhance cellular activity. These findings support the application of *Hibiscus*-infused silica–collagen scaffolds in tissue engineering systems aimed at promoting cell metabolism and biofunctionality.

Keywords: Collagen Hydrogel Scaffolds; Silica Nanoparticles; *Hibiscus sabdariffa* Extract; Cell Metabolism Stimulation; Bioactive Materials; Tissue Engineering; Microstructural Analysis; Porous Topology; Osteogenic Cells; Metabolic Stimulation; Biofuntionality.

1. Introduction

Collagen-based hydrogels have emerged as promising scaffolding systems in tissue engineering due to their excellent biocompatibility, biodegradability, and structural resemblance to the natural extracellular matrix (ECM) [1,2]. Their fibrillar architecture and high-water content make them ideal environments for cell adhesion, proliferation, and differentiation [1,2]. However, native collagen hydrogels often exhibit poor mechanical strength and rapid enzymatic degradation, limiting their functional stability in biomedical applications [3,4]. To overcome these drawbacks, waterborne polyurethane crosslinkers have been employed to enhance the physicochemical properties of collagen scaffolds [5,6]. These crosslinkers can improve structural integrity, resistance to degradation, and mechanical performance, while still maintaining the hydrogel's biocompatibility and porosity—features essential for the incorporation and sustained release of bioactive agents [5,6].

Silica nanoparticles (SiNPs) are widely recognized in biomedical research for their unique structural and surface properties, such as high surface area, tunable porosity, and ease of functionalization [7,8]. Typically synthesized via sol-gel methods—such as the Stöber process [7,8]—SiNPs can be precisely tailored in size, morphology, and surface chemistry. Their porous structure and surface silanol groups make them excellent carriers for drug delivery systems, particularly in applications requiring controlled release and cellular targeting [9]. Recent studies have demonstrated that SiNPs can influence cell metabolism through both direct interactions with cellular components [10], and by serving as delivery vehicles for metabolic modulators [11]. For instance, dexamethasone-loaded SiNPs

embedded in collagen hydrogels have shown enhanced immune cell activation and sustained metabolic stimulation via controlled drug release mechanisms [12]. Beyond synthetic drugs, the high adsorption capacity of SiNPs can be exploited to retain and gradually release phytochemical-rich plant extracts with recognized biological activity. Plant-derived compounds such as curcumin (from Curcuma longa) [13], resveratrol (from grapes) [14], and quercetin (from onions and apples) [15] have been encapsulated in mesoporous SiNPs to modulate oxidative stress, inflammation, and cellular energy metabolism in different tissue models [12-15]. Among these natural sources, *Hibiscus sabdariffa* (commonly known as *hibiscus* or *roselle*) stands out for its rich phytochemical profile, which includes anthocyanins, organic acids, flavonoids, and polyphenols [16-18]. These bioactive compounds have been reported to exhibit antioxidant, anti-inflammatory, and metabolic-regulatory properties, making *hibiscus* extracts attractive candidates for applications in regenerative medicine and metabolic reprogramming [16-18].

Based on this background, the present study hypothesizes that the incorporation of *Hibiscus sabdariffa* extract into SiNPs and their subsequent encapsulation in collagen-based hydrogels will yield bioactive scaffolds capable of stimulating cellular metabolism (Figure 1).

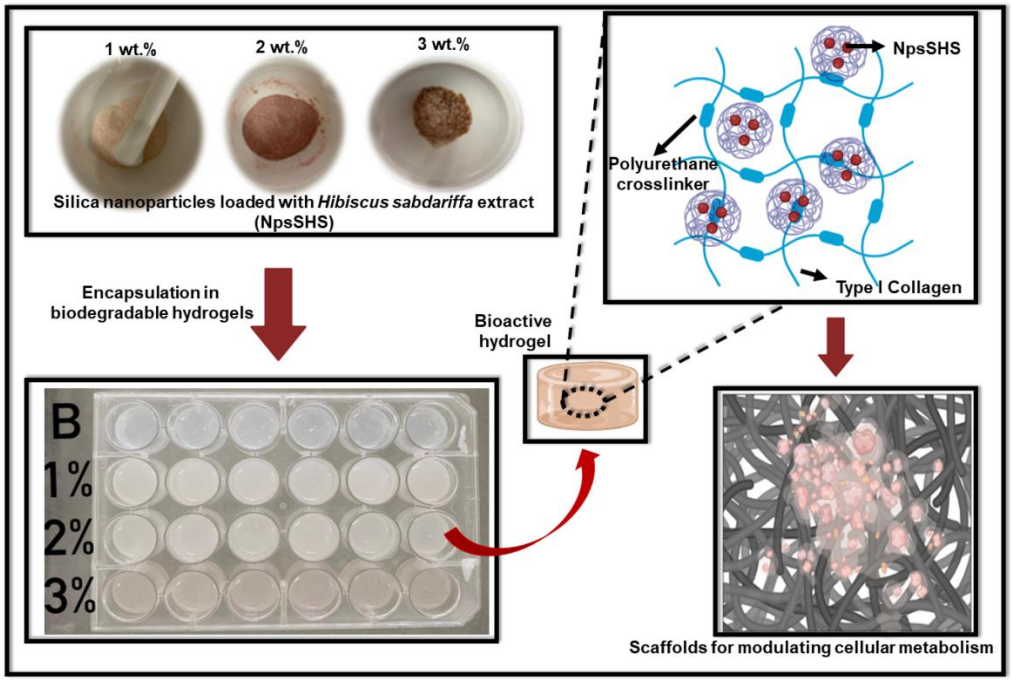

Figure 1. Work hypothesis: Collagen hydrogels with *Hibiscus*-loaded SiNPs enhance scaffold properties and stimulate cell metabolism

This work aims to evaluate how varying the content of *hibiscus* extract (1-3 wt.%) within the SiNPs affects the physicochemical, structural, and biological properties of the resulting scaffolds. In vitro assays will focus on assessing metabolic activity in a range of cell types relevant to soft and hard tissue regeneration, including immune cells, fibroblasts, bone-derived cells and cancer cells.

1.1. Study objectives

The following are the main objectives on this study:

1) To synthesize of *Hibiscus*-loaded Silica Nanoparticles (NpsSHS).

2) To evaluate of physicochemical characterization of NpsSHS-Collagen hydrogels.

3) To analyze the surface microstructure of the biomatrices of collagen-based scaffolds with increasing *Hibiscus*–SiNPs content.

4) To evaluate the thermal stability of composite scalffolds using TGA and DTG analysis.

5) To evaluate the influence of scaffold composition—collagen, SiNPs, and *Hibiscus* extract—on the metabolic activity of different cell types.

2. Materials and Methods

2.1. Preparation of *Hibiscus sabdariffa* extracts

Dried calyces of *Hibiscus sabdariffa* were purchased from a certified local supplier and stored in a desiccator prior to extraction. To prepare the extract, 10 grams of powdered *hibiscus* calyces were accurately weighed and transferred into a 250 mL amber glass flask. A solvent mixture of ethanol: distilled water (70:30 v/v) was added at a ratio of 1:20 (w/v), resulting in 200 mL of total extraction volume. The suspension was stirred continuously at room temperature (25 ± 2 °C) for 24 hours under light-protected conditions to prevent degradation of photosensitive compounds. After extraction, the mixture was filtered through Whatman No. 1 filter paper to remove solid residues. After extraction, the mixture was filtered through Whatman No. 1 filter paper to remove plant residues. The filtrate was then poured into a wide glass container and left to dry at room temperature in a well-ventilated for several days until complete solvent evaporation was achieved. The resulting dry extract was gently scraped, weighed, and stored in airtight containers until further use. This method yielded stable dry extract rich in phytochemicals such as anthocyanins, flavonoids, and organic acids, known for their antioxidant and bioactive properties [19,20].

2.2. Synthesis of *Hibiscus*-loaded Silica Nanoparticles (NpsSHS)

SiNPs containing *Hibiscus sabdariffa* extract were synthesized via a modified Stöber sol-gel method. Tetraethyl orthosilicate (TEOS, 98%, Sigma-Aldrich) was used as the silica precursor. Ethanol (EtOH, CTR Scientific), ammonium hydroxide (NH_4OH, 28–30%, CTR Scientific), and distilled water were used as solvents and catalyst. To prepare the reaction mixture, 80 mL of absolute ethanol were mixed with 10 mL of distilled water and 5 mL of NH_4OH under vigorous magnetic stirring. Once a homogeneous solution was obtained, 5 mL of TEOS were added dropwise to initiate the hydrolysis and condensation reaction.

Separately, *Hibiscus sabdariffa* extract (previously dried and stored) was dissolved in a minimal volume of ethanol and added to the reaction mixture at three different weight ratios relative to the total silica precursor: 1%, 2%, and 3% w/w (NpsSHS1, NpsSHS2, and NpsSHS3, respectively). The reaction was allowed to proceed for 12 hours at room temperature under constant stirring. After the reaction, the resulting nanoparticle suspensions were centrifuged at 5,000 rpm for 15 minutes. The collected precipitates were washed three times with ethanol to remove unreacted extract and reagents. The purified NpsSHS were dried at room temperature in the dark for 48 hours and stored in sealed containers until further use. This method allows for the incorporation of phytochemical compounds into the silica matrix during particle formation, enabling controlled release and bioactivity modulation [21].

2.3. Encapsulation of NpsSHS in collagen hydrogels

Collagen-based hydrogels were prepared by mixing sterile Type I collagen derived from bovine tendon (6 mg/mL in 0.01M hydrochloric acid) [22], phosphate-buffered saline (PBS 10×), a hydrophilic waterborne polyurethane crosslinker, and NpsSHS at different concentrations. The reference hydrogel (B) contained no nanoparticles, while experimental formulations contained the different NpsSHS were formulated. To prepare each formulation, 100 mg of NpsSHS (either 1%, 2%, or 3% loaded) were dispersed in 10 mL of collagen solution under sterile conditions, corresponding to a final concentration of 10 mg/mL of nanoparticles in the hydrogel precursor. The components were gently mixed in sterile culture plates at the proportions listed in Table 1. After homogenization, the culture plates were sealed using sterile adhesive tape and incubated at 37 °C for 24 hours to allow for gelation and crosslinking.

Table 1. Hydrogel formulations with *Hibiscus*-loaded silica nanoparticles

Formulation code	Collagen (mg)	Polyurethane crosslinker (mg)	Type of NpsSHS	Final content of *Hibiscus* extract (µg)
B	6.0 mg	1.8 mg	None	0.0
1%	6.0 mg	1.8 mg	NpsSHS1	100
2%	6.0 mg	1.8 mg	NpsSHS2	200
3%	6.0 mg	1.8 mg	NpsSHS3	300

This encapsulation strategy allows for uniform dispersion of NpsSHS within the collagen matrix and facilitates subsequent evaluation of physicochemical and biological performance [12].

2.4. Physicochemical characterization of NpsSHS-Collagen hydrogels

The physicochemical properties of the collagen hydrogels incorporating *Hibiscus sabdariffa*-loaded silica nanoparticles were assessed using a combination of microstructural, spectroscopic, and thermal techniques. Scanning Electron Microscopy (SEM) was employed to evaluate the surface morphology and nanoparticle dispersion within the hydrogel matrix. Hydrogels were dried at room temperature to form xerogels and subsequently mounted on carbon tape. The analysis was carried out using a JEOL JSM-6510LV/LGS microscope, providing high-resolution images to visualize the integration and distribution of NpsSHS within the fibrillary collagen structure.

Fourier-Transform Infrared Spectroscopy (FTIR) was used to identify functional groups and confirm the successful incorporation of NpsSHS into the collagen-polyurethane hydrogel network. The xerogels were analyzed in ATR mode using a Perkin Elmer Frontier spectrometer. Spectra were recorded over a range of 4000–600 cm^{-1} at a resolution of 16 cm^{-1}, enabling the detection of characteristic interactions between the collagen matrix, polyurethane crosslinker, and phytochemical components from the *Hibiscus* extract. Wide-Angle X-ray Scattering (WAXS) was performed to determine the crystallinity and long-range structural organization of the hydrogels. Samples were dried and analyzed using an Anton Paar SAXS-Emc2 diffractometer equipped with a Cu Kα X-ray source (λ = 1.54 Å). The analysis enabled the identification of semi-crystalline phases and the effect of increasing NpsSHS content on structural ordering.

Ninhydrin Assay was applied to quantify the degree of collagen crosslinking by measuring the availability of free amino groups [5]. Hydrogels from each formulation were incubated with 1 mL of a 1% (w/v) ninhydrin solution in the presence of 3 mL of deionized water. Samples were heated at 90 °C for 30 minutes. After cooling, 200 µL aliquots were transferred into a 96-well plate, and the absorbance was measured at 567 nm using a UV-Vis spectrophotometer (MultiSkan Sky, Thermo Scientific). Crosslinking efficiency was calculated by comparing the absorbance of each formulation with a non-crosslinked collagen control (0%). Swelling Capacity was determined to evaluate the hydrogels' water absorption behavior, which is influenced by the degree of crosslinking and the incorporation of NpsSHS. Hydrogels were weighed before drying (minitial) and then dried at room temperature for 24 h to obtain the xerogel mass (mx). Swelling percentage was calculated using the formula (1):

$$Swelling, (\%) = \left(\frac{m_{initial} - m_x}{m_x}\right) x\ 100 \qquad (1)$$

Thermogravimetric Analysis (TGA) was carried out to examine the thermal stability and degradation profile of the semi-interpenetrating polymer network (semi-IPN) hydrogels. Dried hydrogel samples (~5 mg) were placed in platinum pans and analyzed using a TGA4000 thermogravimetric analyzer (Perkin Elmer). The analysis was conducted under nitrogen atmosphere, with a heating rate of 20 °C/min from 30 to 800 °C. Weight loss (%) was recorded as a function of temperature to identify moisture loss, organic degradation, and residual mass. Additionally, the first derivative thermogravimetric (DTG) curves were calculated to determine the maximum decomposition rate (Tmax) and identify overlapping thermal events. DTG analysis provided precise information on the thermal transitions and decomposition stages associated with the organic matrix, collagen, polyurethane crosslinker, and phytochemicals adsorbed in the NpsSHS. These thermal parameters were compared across the different formulations to evaluate the effect of NpsSHS content on the thermal behavior of the hydrogels.

2.5. Biological evaluation of NpsSHS-collagen hydrogels

The biocompatibility and cytotoxicity of NpsSHS/collagen-based hydrogels were evaluated using different cell types, including human monocytes, porcine fibroblasts, porcine bone-derived cells and human colon cancer cells. Cell cultures were prepared following the methodology described by Caldera-Villalobos et al. (2024) [23], with modifications detailed below.

2.5.1. Cell culture preparation

All cell types were cultured under sterile conditions at 37 °C in a humidified atmosphere containing 5% CO_2. Roswell Park Memorial Institute medium (RPMI) and Dulbecco's Modified Eagle Medium (DMEM) were used as the standard culture medium unless otherwise specified, and was supplemented with 10% fetal bovine serum (FBS) and 1% penicillin-streptomycin (200 µL per 100 mL). Cell concentrations were standardized to 30,000 cells/mL using a Neubauer counting chamber.

2.5.2. Human monocyte isolation and culture

Peripheral blood was obtained from healthy donors. The blood sample was centrifuged at 3000 rpm for 30 minutes to separate plasma, which was discarded. The remaining cellular fraction was washed with (PBS 1x) for 10 minutes,

then resuspended in RPMI-1640 medium (10.44 g/L) supplemented with antibiotics. The monocytes were incubated at 37 °C and reseeded every 48 hours in DMEM to maintain viability [23].

2.5.3. Bone marrow cell Co-Culture

Porcine bone marrow was obtained from freshly slaughtered animals at the local abattoir. A total of 15 g of bone marrow was processed for cell extraction. The tissue was digested proteolytically using a mixture of 60 mL PBS 1x, 10 mL papain, and 2 mL trypsin per 5 g of marrow. The sample was manually ground in a sterile mortar and incubated at 37 °C with continuous agitation for 1 hour. Post-incubation, the suspension was centrifuged at 3000 rpm for 20 minutes. The resulting pellet, containing osteoblasts, osteocytes, and bone marrow stem cells, was resuspended in 45 mL of DMEM supplemented with 500 µL of simulated body fluid (SBF) and 200 µL of antibiotics. The cells were incubated at 37 °C and reseeded every 48 hours in DMEM to maintain viability [24].

2.5.4. Porcine fibroblast isolation

Fibroblasts were isolated from porcine dermis. Skin tissue was cleaned, sectioned, and minced into small fragments, followed by enzymatic digestion using collagenase type I (1 mg/mL) in PBS at 37 °C for 1 hour under gentle agitation. The cell suspension was centrifuged at 2000 rpm for 10 minutes, and the resulting pellet was resuspended in complete DMEM medium. The cells were incubated at 37 °C and reseeded every 48 hours in DMEM to maintain viability [23].

2.5.5. Human colon cancer cells

Colon adenocarcinoma cell line HCT 116 (ATCC® CCL-247™) was used. This cell line was cultured in DMEM supplemented with 10% FBS and 1% antibiotics. Cells were maintained at 37 °C, subcultured at ~80% confluence, and seeded at 30,000 cells/mL for experimental use [25].

2.5.6. Cell Viability Assay

To assess cell viability, 100 mg of each hydrogel formulation were added to wells of 96-well culture plates at a 1:10 ratio with 100 µL of each cell suspension. Cultures were incubated for 24 and 48 hours at 37 °C. PBS-1x was used as a positive control. After the incubation period, 10 µL of 3-(4,5-dimethylthiazol-2-yl)-2,5-diphenyltetrazolium bromide (MTT) solution (5 mg/mL) was added to each well and incubated for 3 hours to allow the formation of formazan crystals by metabolically active cells. Then, 100 µL of propan-2-ol (isopropanol) was added to dissolve the crystals. From this solution, 30 µL was transferred and diluted in 170 µL of fresh isopropanol. Absorbance was measured at 570 nm using a microplate reader (MultiSkan Sky, Thermo Scientific). Metabolic activity was calculated using the following equation (2):

$$Metabolic\ activity, (\%) = \left(\frac{A_{sample}}{A_{control}}\right) x\ 100 \qquad (2)$$

Where Asample is the absorbance of the hydrogel-treated sample, and Acontrol is the absorbance of the control (PBS-1x-treated cells). Viability below 60% was interpreted as cytotoxic, indicating a significant reduction in cellular metabolic activity [23-25].

2.6. Statistical analysis

All experiments were conducted independently in triplicate. Data are expressed as mean values ± standard deviation (SD). To evaluate statistically significant differences between groups, a one-way analysis of variance (ANOVA) was performed, followed by Fisher's Least Significant Difference (LSD) post hoc test for pairwise comparisons. Statistical significance was considered at $p < 0.05$ (*, **).

3. Results and Discussion

3.1. Structural and physicochemical characteristics of the Scaffolds

Figure 2a shows the WAXS diffractograms of collagen hydrogels incorporating silica nanoparticles loaded with *Hibiscus sabdariffa* extract (NpsSHS).

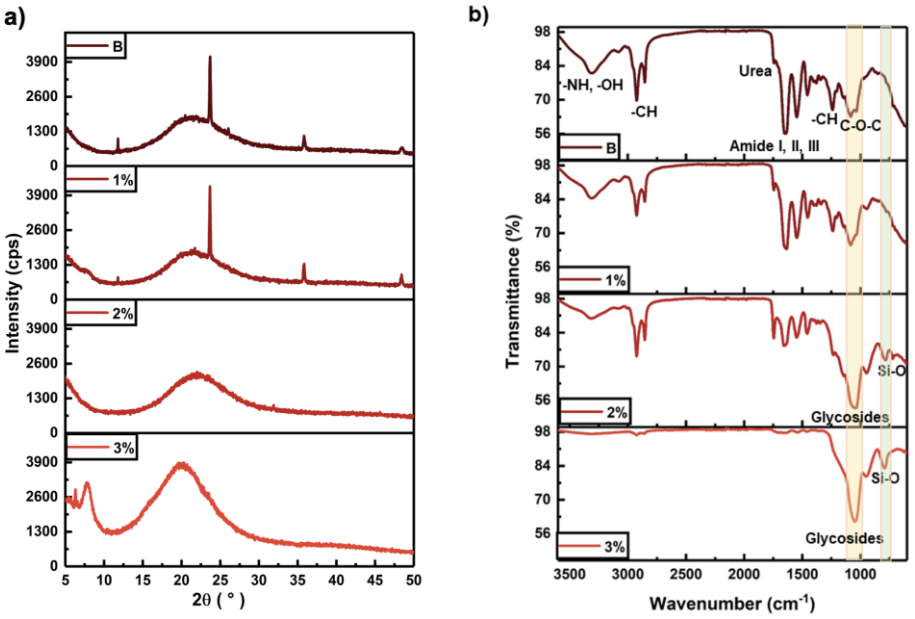

Figure 2. (a) WAXS patterns showing structural transitions, and (b) FTIR spectra of collagen hydrogels with *Hibiscus sabdariffa* extract-SiNPs

The scaffold without SiNPs (B) exhibits a characteristic broad amorphous halo centered around 22°, along with crystalline signals at 12°, 24°, 35.5°, and 48°, which are attributed to the ordered fibrillar architecture of type I collagen derived from bovine tendon [26]. As the concentration of *Hibiscus* extract increases within the fibrillar matrix, a progressive reduction in the intensity of collagen's crystalline reflections is observed, particularly in the 1% scaffold. This suggests that short-range interactions (e.g., hydrogen bonding) between polyphenolic/glycosidic phytochemicals and collagen's polar groups disrupt molecular ordering. At higher extract contents (2% and 3%), the crystalline features associated with collagen disappear entirely. Instead, two broad amorphous halos appear, centered at approximately 8° and 20°, corresponding to the disordered, mesoporous silica network formed through the sol-gel synthesis process. These halos are attributed to the mesoporous silica framework, suggesting the incorporation of silica with an ordered mesostructure, potentially resembling MCM-41 or SBA-15 type materials [27]. These findings indicate that the increasing incorporation of *Hibiscus* interferes with the self-assembly and crystallinity of the collagen fibrils, promoting the formation of a hybrid amorphous matrix. Such molecular-level

disorganization may influence both the mechanical properties and the bioactivity of the scaffold, offering potential benefits for modulating cell–matrix interactions and metabolic responses [23].

Based on the WAXS structural data, the presence of a semicrystalline organization in scaffolds containing NpsSHS1 suggests the formation of an internal network with higher molecular order, induced by the integration of mesoporous silica nanoparticles. The development of such ordered domains is likely due to interactions between the silica surface and collagen fibrils, which promote local alignment or reinforcement within the polymeric matrix. This molecular-level organization not only reflects improved structural definition but also could lead to distinct physicochemical properties—such as increased surface area, stiffness, and diffusional control—that can significantly influence cell–material interactions [28]. In the context of biomedical applications, scaffolds with semicrystalline/amorphous features offer a promising strategy for modulating cellular metabolism [29]. The increased surface order and mesoporosity associated with silica nanoparticles can enhance the adsorption and gradual release of bioactive molecules of *Hibiscus*, thus creating a microenvironment that supports regulated metabolic responses. Furthermore, these structural features may influence cell behavior through mechanotransduction pathways, affecting mitochondrial activity, proliferation, or differentiation depending on the cell type [30]. Therefore, the design of scaffolds with molecularly ordered architectures represents a valuable tool in engineering platforms aimed at metabolic regulation and functional tissue regeneration.

Figure 2b shows the FTIR spectra highlighting the main functional groups present in the scaffolds. The pure collagen hydrogel (B) exhibits characteristic stretching vibrations of –OH and –NH groups at ~3600 cm^{-1}, aliphatic –CH at ~2700 cm^{-1}, and a urea linkage band at 1720 cm^{-1}. The latter arises from the reaction between primary amine groups on collagen fibrils and terminal isocyanate groups from the polyurethane crosslinker [5]. Additionally, the spectra display the amide I (~1650 cm^{-1}), amide II (~1560 cm^{-1}), and amide III (~1480 cm^{-1}) vibrations corresponding to peptide bonds within the collagen structure [23,29]. The in-plane deformation of –CH bonds, especially abundant in proline and hydroxyproline residues, appears at 1240 cm^{-1}, while the ether C–O–C stretching vibration at 1100 cm^{-1} is associated with the polyurethane network [5,23,29].

As the content of *Hibiscus sabdariffa* extract increases within the fibrillar scaffold, a progressive decrease in the intensity of the –OH, –NH, –CH, urea, and amide I–III bands is observed. This suggests the formation of hydrogen bonds between the polyphenolic and flavonoid constituents of the extract and the collagen matrix, altering the vibrational modes of the protein. Notably, the scaffold containing 3 wt.% extract shows a significant enhancement of the band at ~1100 cm^{-1}, which corresponds to glycosidic C–O stretching. This indicates the presence of a high concentration of bioactive glycosides, such as hibiscoside, delphinidin-3-sambubioside, and cyanidin-3-sambubioside, all known for their antioxidant and anti-inflammatory activities [16-18]. Furthermore, scaffolds with NpsSHS2 y NpsSHS3 exhibit a distinct band at ~780 cm^{-1}, assigned to Si–O–Si stretching vibrations, confirming the successful incorporation and homogeneous dispersion of mesoporous silica nanoparticles within the collagen matrix.

The attenuation of characteristic collagen vibrational bands in the FTIR spectra—especially those related to amide linkages and polar groups—suggests the formation of non-covalent interactions, likely involving hydrogen bonding

and π–π stacking between collagen fibrils and phytochemicals such as polyphenols, flavonoids, and glycosides. This molecular reorganization aligns with the WAXS profiles, which demonstrate a progressive transition from a partially ordered to a predominantly amorphous structure as the *Hibiscus* extract content increases. This shift implies a disordered, yet stabilized, network driven by short-range interactions. Such molecular-level structuring is particularly relevant for influencing the diffusion of bioactive compounds and the spatial presentation of biochemical cues. These scaffold characteristics are advantageous for modulating cellular metabolism, as they contribute to a tunable microenvironment that regulates the availability of nutrients, signaling molecules, and mechanical stimuli—all of which critically affect cell proliferation, differentiation, and metabolic activity [5, 23,29].

Microstructural characteristics of the scaffolds, as analyzed by SEM, are shown in Figure 3a. The control collagen hydrogel without NpsSHS exhibits a porous fibrillar morphology typical of type I collagen-based hydrogels.

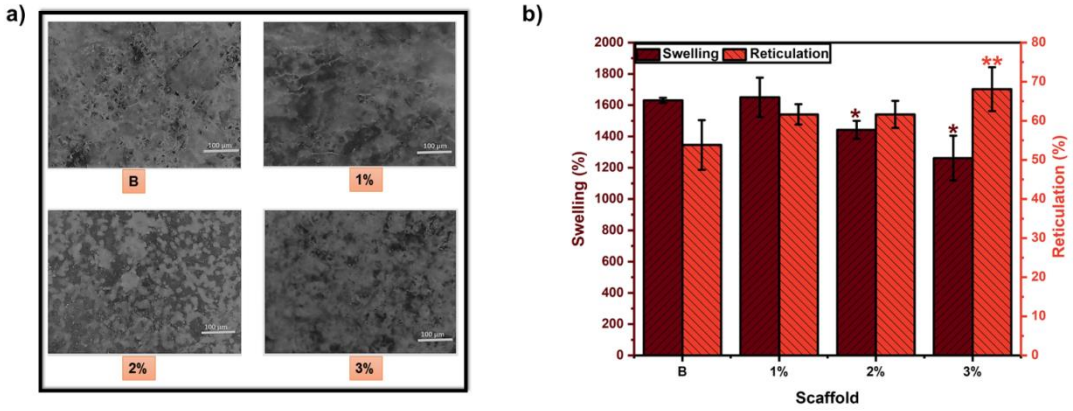

Figure 3. (a) SEM images showing surface morphology of collagen-based scaffolds with increasing *Hibiscus*–SiNPs content, and (b) swelling ratio and crosslinking index profiles

As the concentration of *Hibiscus sabdariffa* extract increases (1–3 wt%), distinct surface features emerge. The NpsSHS1 scaffold (1 wt%) shows disorganized fibrillar alignment with visibly thicker fibers compared to B, consistent with the decreased intensity of the crystalline signals associated with the collagen fibrillar structure in WAXS patterns. This scaffold also exhibits increased surface porosity. The 2% scaffold (NpsSHS2) displays spherical nanoparticles distributed on a reduced fibrillar matrix, suggesting that the NpsSHS are embedded and homogeneously dispersed within the collagen network. This dispersion is likely facilitated by short-range interactions revealed by FTIR and WAXS. In the 3% scaffold (NpsSHS3), the spherical morphology of the SiNPs becomes less defined due to encapsulation by phytochemical components of the *Hibiscus sabdariffa* extract—particularly glycosides, exhibiting an increasingly amorphous character. This scaffold also presents an interconnected porous structure favorable for mass transport and biological integration. These microstructural findings support the potential of these scaffolds for modulating cellular metabolism. The observed increase in surface porosity, fiber rearrangement, and the homogeneous distribution of SiNPs—especially in the presence of glycoside-rich phytochemicals—enhance the scaffold's surface area and chemical functionality. These features can facilitate nutrient exchange, support selective molecular interactions, and create favorable microenvironments that influence cell adhesion, signaling, and metabolic activity [5,23,29]. The interconnected porous network observed in

the 3% scaffold, combined with the presence of bioactive compounds, may further promote sustained metabolic stimulation, making these systems promising for bioactive scaffold design in tissue engineering.

The swelling profiles of the scaffolds are shown in Figure 3b. Swelling capacities of 1660%, 1680%, 1490%, and 1295% were recorded for B, 1%, 2%, and 3%, respectively. Statistically significant differences were observed when comparing the swelling of scaffold B to those containing higher concentrations of NpsSHS (2% and 3%), indicating that the increased incorporation of *Hibiscus sabdariffa* extract into the fibrillar matrix tends to reduce the scaffold's water absorption capacity. This behavior may be attributed to the presence of occluded NpsSHS aggregates enriched with phytochemicals, where the hydrocarbon-rich regions of the extract generate partial hydrophobic zones that hinder water uptake. Additionally, the progressive loss of molecular ordering and increased amorphous character, as evidenced by WAXS, suggest a disruption of the native collagen fibrillar architecture. This disorganization likely results in tighter entanglement of the matrix components and reduced free volume, which in turn limits the scaffold's ability to swell [5,23,29]. Nevertheless, all scaffolds exhibited swelling capacities above 1200%, highlighting their excellent water absorption potential and suitability for applications requiring highly hydrophilic and biofunctional biomaterials. These results highlight how the modulation of swelling behavior through *Hibiscus sabdariffa* extract incorporation may be leveraged to influence cellular metabolic responses. The reduced swelling ratio observed in the 2% and 3% scaffolds suggests a denser and more compact amorphous microenvironment. This structural rearrangement may hinder water uptake and restrict the diffusion of nutrients and metabolic waste, as well as alter localized mechanical cues—all of which are critical regulators of cellular metabolism [31]. Moreover, the presence of phytochemical-enriched regions with controlled hydrophilicity provides a tunable interface that can modulate hydration layers and interfacial interactions with cell membranes [32]. This structural control opens new possibilities for designing scaffolds that direct specific metabolic pathways through the engineered regulation of water transport and biochemical microenvironments.

Crosslinking indices of the scaffolds are shown in Figure 3b, revealing values of 55%, 63%, 64%, and 68% for scaffolds B, 1%, 2%, and 3%, respectively. A statistically significant increase in crosslinking was observed in the 3% scaffold compared to B. This enhancement is attributed to short-range interactions between phytochemical components of the *Hibiscus sabdariffa* extract and polar groups present on collagen fibers. These interactions likely involve hydrogen bonding and van der Waals forces, which promote additional physical crosslinking beyond the covalent urea bonds formed with the polyurethane network. Moreover, the increased amorphous character observed in scaffolds with higher extract content suggests a disordered yet compact molecular arrangement that may stabilize the network through dense packing and non-covalent interactions. Together, these findings demonstrate that phytochemical incorporation not only modulates chemical functionality but also contributes to improved scaffold structural integrity by reinforcing inter- and intramolecular interactions within the fibrillar matrix. These crosslinking results align with the microstructural features observed in SEM analysis. As the content of *Hibiscus sabdariffa* extract increases, the scaffolds exhibit reduced fibrillar definition, more compact morphologies, and the appearance of spherical SiNP-rich domains—particularly evident in the 2% and 3% scaffolds. These morphological changes support the presence of enhanced crosslinking and localized molecular densification, as phytochemical-rich regions promote entrapment of SiNPs and restrict collagen fiber mobility. Although WAXS analysis indicates

a transition toward a more amorphous structure, this disordered molecular arrangement is likely stabilized through dense packing and short-range interactions, such as hydrogen bonding and π–π stacking. In the context of cellular metabolism control, the higher crosslinking degree and resulting structural compaction can modulate the scaffold's permeability to nutrients, signaling molecules, and metabolic byproducts—ultimately offering a tunable microenvironment for directing cellular responses such as proliferation, differentiation, and metabolic activation [33]. Figure 4a shows the TGA thermograms of the scaffolds.

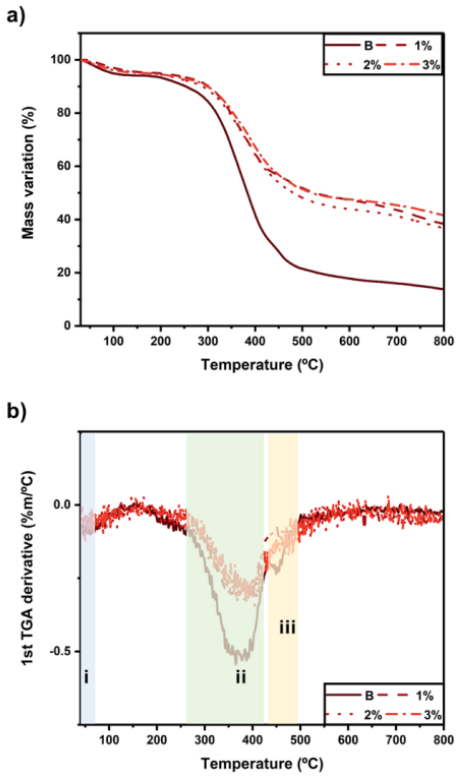

Figure 4. TGA (a) and DTG (b) thermograms of scaffolds with increasing *Hibiscus* extract content

All biomaterials exhibit three distinct mass loss regions: (i) the evaporation of water physically entrapped within the matrix, observed between 30–110 °C; (ii) the endothermic degradation of the scaffold's polymeric components and the phytochemicals present in the *Hibiscus* extract, occurring between 300–500 °C; and (iii) the exothermic degradation of residual components, observed between 600–800 °C. The encapsulation of SiNPs with *Hibiscus* extract reduces the thermal degradation of the scaffolds, suggesting that short-range interactions between NpsSHS and type I collagen fibers enhance the thermal stability of the composite. Notably, scaffolds containing 3 wt.% of *Hibiscus* extract exhibited the highest thermal resistance, as evidenced by a small final residual mass. The residual mass increased proportionally with the content of *Hibiscus* extract in the scaffolds, with values of 11%, 42%, 41%, and 44% for B, and formulations with 1%, 2%, and 3% of *Hibiscus* extract, respectively. The formation of amorphous matrices likely facilitates heat transfer and dissipation, thereby contributing to improved resistance against thermal degradation.

Figure 4b displays the DTG curves, which reveal the temperatures at which maximum decomposition of the chemical components within the scaffolds occurs. In general, water molecules and volatile compounds from the *Hibiscus* extract are evaporated at a maximum temperature of approximately 90 °C (region i in the DTG curve). In

the endothermic decomposition region, two distinct degradation peaks can be observed: one with a maximum at 376 °C (region ii), corresponding to the degradation of collagen and phytochemicals such as glycosides and polyphenols; and a second peak at 470 °C (region iii), associated with the thermal degradation of the polyurethane. Notably, the area under the endothermic degradation peaks is larger for the scaffold without NpsSHS, indicating greater mass loss. In contrast, the formulations containing NpsSHS show reduced peak areas, suggesting that hydrogen bonding and van der Waals interactions between the SiNPs, phytochemicals, and the fibrillar matrix play a critical role in reducing thermal decomposition and enhancing scaffold stability. The enhanced thermal stability observed in scaffolds containing NpsSHS not only indicates greater resistance to structural degradation but also suggests a more controlled and sustained release of the bioactive compounds from the *Hibiscus* extract [34]. This gradual release can more effectively modulate the scaffold's microenvironment, allowing for precise regulation of cellular metabolism—particularly important in applications aimed at promoting regenerative processes or minimizing inflammatory responses [35]. Therefore, these thermally stable scaffolds represent a promising platform for tissue engineering and advanced therapeutic applications, where both structural integrity and controlled bioactive delivery are essential for eliciting a favorable biological response [34, 35].

3.2. Influence of scaffold composition on cell metabolism

Figure 5 shows the results of evaluating the influence of scaffold composition—collagen, SiNPs, and *Hibiscus* extract—on the metabolic activity of different cell types.

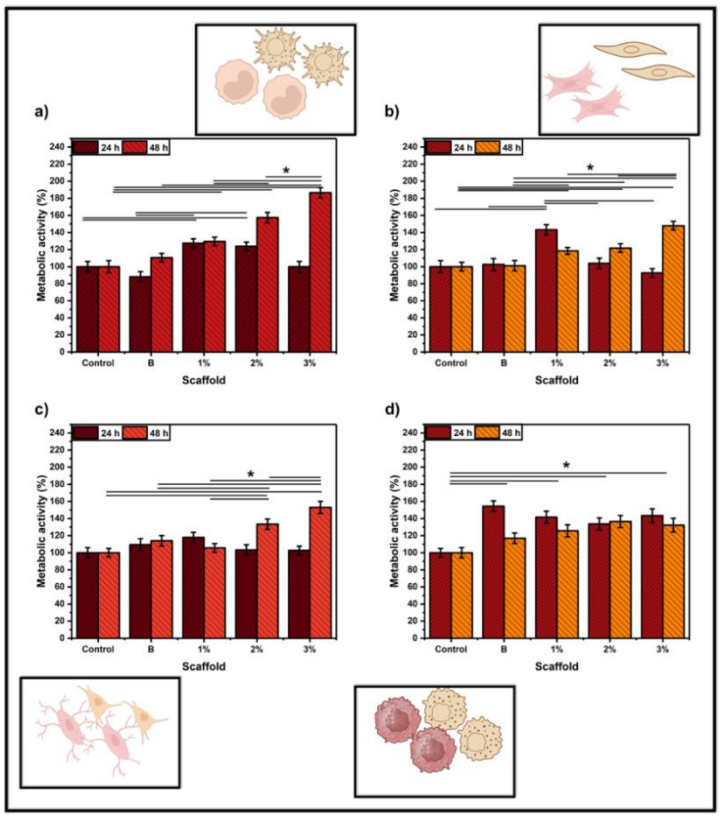

Figure 5. Mitochondrial function of different cell types cultured on collagen-based scaffolds with SiNPs and *Hibiscus* extract at 24 and 48 hours: a) monocytes, b) fibroblasts, c) bone marrow-derived cells, and d) colon cancer cells

For monocytes (Figure. 5a), after 24 hours, metabolic activity values above 80% were recorded for all conditions, indicating no cytotoxic effects. Statistically significant differences were observed for the 1% and 2% scaffolds compared to the control, B, and 3% groups, suggesting that intermediate concentrations of *Hibiscus* extract (1% and 2%) enhance monocyte metabolic activity at this early time point. After 48 hours, a notable increase in metabolic activity was observed in monocytes cultured on NpsSHS-containing scaffolds, reaching up to 183% compared to the control (3%).

These results indicate that higher *Hibiscus* extract content further promotes metabolic stimulation over time. This improvement is promoted by the amorphous characteristics of the matrices with high *Hibiscus* extract content. The enhanced mitochondrial function of monocytes in response to scaffolds containing NpsSHS can be attributed to the synergistic effects of the *Hibiscus* phytochemicals and the silica nanoparticles.

The bioactive compounds present in the extract—such as polyphenols and glycosides—are known to possess immunomodulatory and antioxidant properties, which can promote cell activation and survival [16-18]. Additionally, the presence of SiNPs contributes to improved scaffold stability and provides favorable surface interactions that support cell adhesion and signaling [9-15]. Together, these factors create a bioactive microenvironment that not only preserves cell viability but actively stimulates cellular metabolism. This response is particularly relevant for biomedical applications involving immune regulation and tissue repair, such as in wound healing or inflammatory modulation, where enhancing monocyte activity can accelerate the initiation of regenerative processes [36].

Fibroblasts cultured on these scaffolds (Figure 5b) exhibited metabolic activity comparable to the control at 24 hours; however, the 1% formulation showed a statistically significant increase in metabolic activity compared to the other groups. This effect is likely due to the fibrillar structure of the scaffold, which actively supports fibroblast function and facilitates the uptake of phytochemicals from the *Hibiscus* extract. After 48 hours, no cytotoxic effects were observed, and a stimulation of fibroblast metabolic activity was evident in all scaffolds containing *Hibiscus* extract, following a concentration-dependent trend. Significant differences were found in the mitochondrial function of fibroblasts grown on the 2% and 3% scaffolds compared to both the control and the extract-free scaffold, indicating that higher extract content enhances cellular activation over time. The fibrillar matrix promotes fibroblast adhesion, alignment, and growth, which in turn stimulates cellular metabolism [5,23,25]. Additionally, the phytochemicals in the extract, such as polyphenols and glycosides, contribute to this metabolic boost by influencing cellular signaling pathways that promote proliferation and ECM production [16-18]. At higher extract concentrations (2% and 3%), the increased presence of these bioactive molecules further enhances fibroblast activity, likely accelerating tissue regeneration processes [37]. These findings are highly relevant to biomedical applications, especially in tissue engineering and wound healing, where fibroblasts play a key role in collagen synthesis and tissue repair [38]. By improving fibroblast activity and promoting ECM formation, these scaffolds may significantly enhance the effectiveness of regenerative therapies.

Bone marrow-derived cells (Figure 5c) showed mitochondrial function comparable to the control after 24 hours, indicating no cytotoxic effects across all scaffold formulations. However, no statistically significant differences

were detected at this early time point. After 48 hours of culture, a marked stimulation of metabolic activity was observed in cells grown on scaffolds containing higher concentrations of *Hibiscus* extract (2% and 3%) (up 155%).

These values were significantly greater than those for the 1%, B, and control groups, highlighting a positive correlation between extract content and cellular metabolic activation in bone-derived cells. The enhanced mitochondrial function observed in bone marrow-derived cells after 48 hours, particularly in scaffolds containing higher concentrations of *Hibiscus* extract (2% and 3%), suggests a time- and dose-dependent bioactivation effect. This improvement can be attributed to the bioactive phytochemicals in the extract, which may promote osteogenic cell function through antioxidant and anti-inflammatory mechanisms, as well as by modulating signaling pathways involved in cellular proliferation and differentiation [16-18]. The fibrillar scaffold structure further facilitates cell–material interactions, enhancing nutrient diffusion and cellular anchorage. These findings are particularly relevant for bone tissue engineering and regenerative medicine, where early metabolic activation of progenitor cells is critical for subsequent differentiation, matrix deposition, and bone remodeling [33,39]. Thus, incorporating phytochemical-rich extracts into bioengineered scaffolds offers a promising strategy for developing bioactive materials capable of supporting and accelerating bone repair.

Finally, the response of human colon cancer cells was evaluated (Figure 5d). At 24 hours, the scaffold without NpsSHS (B) significantly stimulated the metabolic activity of these cancer cells compared to both the control and the NpsSHS-containing formulations. However, no cytotoxic effects or reduction in mitochondrial function were observed in the presence of NpsSHS. After 48 hours, a slight decrease in metabolic activity was recorded across all treatments, but again without signs of cytotoxicity. Interestingly, scaffolds containing *Hibiscus* extract and SiNPs still induced significantly higher metabolic activity than the control. Despite the known antioxidant properties of polyphenolic compounds present in the extract, no inhibitory effect on cancer cell metabolism was detected under the conditions tested. This lack of inhibitory effect may be due to insufficient concentration, limited bioavailability, or rapid metabolic adaptation of cancer cells to phytochemicals in the scaffold [40]. To enhance the therapeutic potential of these scaffolds for anticancer applications, future strategies could involve the incorporation of higher doses or more potent phytochemical fractions from *Hibiscus*, combination with known chemotherapeutic agents or photosensitizers for synergistic effects [41], or the design of stimuli-responsive scaffolds that release bioactive molecules in response to tumor-specific microenvironmental cues (e.g., pH, enzymes, redox conditions) [41]. Additionally, surface modification of SiNPs to improve selective cellular uptake by cancer cells or to co-deliver gene-silencing agents (e.g., siRNA) could further improve efficacy [42,43]. These approaches could transform the scaffold system into a multifunctional platform capable of both supporting tissue regeneration and providing localized anticancer therapy with reduced systemic toxicity.

4. Conclusions

This study demonstrated the successful development of bioactive and structurally reinforced collagen-based scaffolds through the incorporation of silica nanoparticles loaded with *Hibiscus sabdariffa* extract. The increase in extract content led to the formation of amorphous matrices with enhanced thermal stability, higher crosslinking density, and highly absorbent behavior. The phytochemical–collagen interactions played a key role in improving

the physicochemical properties of the scaffolds. Importantly, the in vitro results confirmed that these hybrid scaffolds significantly stimulated the metabolic activity of immune, connective, and bone cells, particularly at higher concentrations of the extract. Although no cytotoxic effects were observed on colon cancer cells, the system showed no inhibitory impact either, indicating the need for further functionalization to enable selective anticancer responses. Overall, the findings validated the potential of these scaffolds as a versatile platform for promoting cell activity and supporting regenerative processes, offering a promising foundation for future applications in tissue engineering and phytochemical-based therapeutic strategies.

5. Future Suggestions

The following are some future suggestions of this present study:

(1) To target anticancer functionalization.

(2) To study and optimize the release of *H. sabdariffa* extract from silica nanoparticles within the hydrogel matrix.

(3) To study immunodulatory response of the hydrogel in relevant animal model.

(4) To study the rheology of hydrogels.

(5) To study the drug release of the hydrogels of *H. sabdariffa*.

Declarations

Source of Funding

This study did not receive any grant from funding agencies in the public or not-for-profit sectors.

Competing Interests Statement

The authors declare that they have no conflict of interest.

Consent for publication

The authors declare that they consented to the publication of this study.

Authors' contributions

All the authors took part in literature review, analysis, and manuscript writing equally.

Informed Consent

Not applicable.

References

[1] Antoine, E.E., Vlachos, P.P., & Rylander, M.N. (2014). Review of collagen I hydrogels for bioengineered tissue microenvironments: characterization of mechanics, structure, and transport. Tissue Engineering, Part B, Reviews, 20(6): 683–96. https://doi.org/10.1089/ten.teb.2014.0086.

[2] Pires Figueiredo, M., Rodríguez-Fernández, S., Copes, F., & Mantovani, D. (2025). Review of collagen type I-based hydrogels: focus on composition-structure-properties relationships. NPJ Biomedical Innovations, 2(1): 16. https://doi.org/10.1038/s44385-025-00018-w.

[3] Ho, T.C., Chang, C.C., Chan, H.P., Chung, T.W., Shu, C.W., Chuang, K.P., Duh, T.H., Yang, M.H., & Tyan, Y.C. (2022). Hydrogels: Properties and Applications in Biomedicine. Molecules, 27(9): 2902. https://doi.org/10.3390/molecules27092902.

[4] Zhang, X., Liang, Y., Luo, D., Li, P., Chen, Y., Fu, X., Yue, Y., Hou, R., Liu, J., & Wang, X. (2024). Advantages and disadvantages of various hydrogel scaffold types: A research to improve the clinical conversion rate of loaded MSCs-Exos hydrogel scaffolds. Biomedicine & Pharmacotherapy, 179: 117386. https://doi.org/10.1016/j.biopha.2024.117386.

[5] Claudio-Rizo, J.A., Mendoza-Novelo, B., Delgado, J., Castellano, L.E., & Mata-Mata, J.L. (2016). A new method for the preparation of biomedical hydrogels comprised of extracellular matrix and oligourethanes. Biomedical materials (Bristol, England), 11(3): 035016. https://doi.org/10.1088/1748-6041/11/3/035016.

[6] León-Campos, M.I., Claudio-Rizo, J.A., Cabrera-Munguía, D.A., Cobos-Puc, L.E., Caldera-Villalobos, M., González-Díaz, M.O., & Enríquez-Medrano, F.J. (2024). Development of novel bioactive waterborne polyurethanes: Effect of polyurethane chemical structure on its properties. Journal of Polymer Research, 31(7): 213. https://doi.org/10.1007/s10965-024-04055-8.

[7] Janjua, T.I., Cao, Y., Kleitz, F., Linden, M., Yu, C., & Popat, A. (2023). Silica nanoparticles: A review of their safety and current strategies to overcome biological barriers. Advanced Drug Delivery Reviews, 203: 115115. https://doi.org/10.1016/j.addr.2023.115115.

[8] Akhter, F., Rao, A.A., Abbasi, M.N., Wahocho, S.A., Mallah, M.A., Anees-ur-Rehman, H., & Chandio, Z.A. (2022). A Comprehensive Review of Synthesis, Applications and Future Prospects for Silica Nanoparticles (SNPs). Silicon, 14(14): 8295–8310. https://doi.org/10.1007/s12633-021-01611-5.

[9] She, X., Chen, L., Yi, Z., Li, C., He, C., Feng, C., Wang, T., Shigdar, S., Duan, W., & Kong, L. (2018). Tailored Mesoporous Silica Nanoparticles for Controlled Drug Delivery: Platform Fabrication, Targeted Delivery, and Computational Design and Analysis. Mini Reviews in Medicinal Chemistry, 18(11): 976–989. https://doi.org/10.2174/1389557516666160505114814.

[10] Susnik, E., Taladriz-Blanco, P., Drasler, B., & Balog, S. (2020). Increased Uptake of Silica Nanoparticles in Inflamed Macrophages but Not upon Co-Exposure to Micron-Sized Particles. Cells, 9(9). https://doi.org/10.3390/cells9092099.

[11] Awashra, M., & Młynarz, P. (2023). The toxicity of nanoparticles and their interaction with cells: an in vitro metabolomic perspective. Nanoscale Advances, 5(10): 2674–2723. https://doi.org/10.1039/d2na00534d.

[12] Rangel-Argote, M., Claudio-Rizo, J.A., Castellano, L.E., Vega-González, A., Mata-Mata, J.L., & Mendoza-Novelo, B. (2017). ECM–oligourethene–silica hydrogels as a local drug release system of dexamethasone for stimulating macrophages. RSC Advances, 7(17): 10443–10453. https://doi.org/10.1039/c6ra25989h.

[13] Maleki Dizaj, S., & Sharifi, S. (2022). Curcumin-Loaded Silica Nanoparticles: Applications in Infectious Disease and Food Industry. Nanomaterials, 12(16). https://doi.org/10.3390/nano12162848.

[14] Gu, Y., & Fei, Z. (2022). Mesoporous Silica Nanoparticles Loaded with Resveratrol Are Used for Targeted Breast Cancer Therapy. Journal of Oncology, 8471331. https://doi.org/10.1155/2022/8471331.

[15] Catauro, M., Papale, F., Bollino, F., Piccolella, S., Marciano, S., Nocera, P., & Pacifico, S. (2015). Silica/ quercetin sol-gel hybrids as antioxidant dental implant materials. Science and Technology of Advanced Materials, 16(3): 035001. https://doi.org/10.1088/1468-6996/16/3/035001.

[16] Da-Costa-Rocha, I., Bonnlaender, B., Sievers, H., Pischel, I., & Heinrich, M. (2014). *Hibiscus sabdariffa* L. - a phytochemical and pharmacological review. Food Chemistry, 165: 424–43. https://doi.org/10.1016/j.foodchem. 2014.05.002.

[17] Riaz, G., & Chopra, R. (2018). A review on phytochemistry and therapeutic uses of *Hibiscus sabdariffa* L. Biomedicine & Pharmacotherapy = Biomedecine & Pharmacotherapie, 102: 575–586. https://doi.org/10.1016/j.bio pha.2018.03.023.

[18] Hamrita, B., Emira, N., Papetti, A., Badraoui, R., Bouslama, L., Ben Tekfa, M.I., Hamdi, A., Patel, M., Elasbali, A.M., Adnan, M., Ashraf, S.A., & Snoussi, M. (2022). Phytochemical Analysis, Antioxidant, Antimicrobial, and Anti-Swarming Properties of *Hibiscus sabdariffa* L. Calyx Extracts. In Vitro and In Silico Modelling Approaches, Evidence-Based Complementary and Alternative Medicine, (1): 1252672. https://doi.org/ 10.1155/2022/1252672.

[19] Villalobos-Vega, M.J., Rodríguez-Rodríguez, G., Armijo-Montes, O., & Jiménez-Bonilla, P. (2023). Optimization of the Extraction of Antioxidant Compounds from Roselle Hibiscus Calyxes (*Hibiscus sabdariffa*), as a Source of Nutraceutical Beverages. Molecules, 28(6). https://doi.org/10.3390/molecules28062628.

[20] Carvajal-Zarrabal, O., Hayward-Jones, P.M., Orta-Flores, Z., Nolasco-Hipólito, C., Barradas-Dermitz, D.M., Aguilar-Uscanga, M.G., & Pedroza-Hernández, M.F. (2009). Effect of *Hibiscus sabdariffa* L. dried calyx ethanol extract on fat absorption-excretion, and body weight implication in rats. Journal of Biomedicine & Biotechnology, 394592. https://doi.org/10.1155/2009/394592.

[21] Rahman, I.A., Vejayakumaran, P., Sipaut, C.S., Ismail, J., Bakar, M.A., Adnan, R., & Chee, C.K. (2007). An optimized sol–gel synthesis of stable primary equivalent silica particles. Colloids and Surfaces A: Physicochemical and Engineering Aspects, 294(1): 102–110. https://doi.org/10.1016/j.colsurfa.2006.08.001.

[22] Claudio-Rizo, J.A., Rangel-Argote, M., Castellano, L.E., Delgado, J., Mata-Mata, J.L., & Mendoza-Novelo, B. (2017). Influence of residual composition on the structure and properties of extracellular matrix derived hydrogels. Materials Science & Engineering. C, Materials for Biological Applications, 79: 793–801. https://doi.org/10.1016/j. msec.2017.05.118.

[23] Caldera-Villalobos, M., Cabrera-Munguía, D.A., Becerra-Rodríguez, J.J., & Claudio-Rizo, J.A. (2022). Tailoring biocompatibility of composite scaffolds of collagen/guar gum with metal–organic frameworks. RSC Advances, 12(6): 3672–3686. https://doi.org/10.1039/d1ra08824f.

[24] Varguez-Catzim, P., Hernández-Aburto, M., Rodriguez-Canto, W., Hunh-Ibarra, M., Aguilar-Vega, M., Claudio-Rizo, J.A., & González-Díaz, M.O. (2025). Tailoring membrane technology with galactomannan for

enhanced biocompatibility and antibacterial action. International Journal of Biological Macromolecules, 286: 138320. https://doi.org/10.1016/j.ijbiomac.2024.138320.

[25] Usme-Duque, L.K., Claudio-Rizo, J.A., Nuncio-Esquivel, J.A., León-Campos, M.I., Cruz-Requena, M., Ríos-González, L.J., Ascacio- Valdés, J.A., & Medina-Morales, M.A. (2025). Optimization of fungal fermentation for the extraction of polyphenols from *Flourensia cernua* and its effect on cellular metabolism. Journal of Biotechnology, 401: 60–73. https://doi.org/10.1016/j.jbiotec.2025.02.011.

[26] Ata, O., Bakar, B., Turkoz, B.K., Kumcuoglu, S., Aydogdu, Y., Gumustas, B., Doganay, G.D., Basturk, E., & Tavman, S. (2024). Structural and molecular characterization of collagen-type I extracted from lamb feet. Journal of Food Science, 89(1): 330–341. https://doi.org/10.1111/1750-3841.16870.

[27] Tanev, P.T., & Pinnavaia, T.J. (1995). A Neutral Templating Route to Mesoporous Molecular Sieves. Science, 267(5199): 865–867. https://doi.org/10.1126/science.267.5199.865.

[28] Kołbuk, D., Ciechomska, M., Jeznach, O., & Sajkiewicz, P. (2022). Effect of crystallinity and related surface properties on gene expression of primary fibroblasts. RSC Adv., 12(7): 4016–4028. https://doi.org/10.1039/d1ra07237d.

[29] Amaya-Chantaca, N.J., Caldera-Villalobos, M., & Claudio-Rizo, J.A. (2023). Semi-IPN hydrogels of collagen and gum arabic with antibacterial capacity and controlled release of drugs for potential application in wound healing. Progress in Biomaterials, 12(1): 25–40. https://doi.org/10.1007/s40204-022-00210-w.

[30] Chen, L., Zhou, X., & He, C. (2019). Mesoporous silica nanoparticles for tissue-engineering applications. WIREs Nanomedicine and Nanobiotechnology, 11(6): e1573. https://doi.org/10.1002/wnan.1573.

[31] Huang, G., Li, F., Zhao, X., Ma, Y., Li, Y., & Lin, M. (2017). Functional and Biomimetic Materials for Engineering of the Three-Dimensional Cell Microenvironment. Chemical Reviews, 117(20): 12764–12850. https://doi.org/10.1021/acs.chemrev.7b00094.

[32] Damodaran, S. (2015). Water at Biological Phase Boundaries: Its Role in Interfacial Activation of Enzymes and Metabolic Pathways. Sub-Cellular Biochemistry, 71: 233–61. https://doi.org/10.1007/978-3-319-19060-0_10.

[33] Eivazzadeh-Keihan, R., Chenab, K.K., Taheri-Ledari, R., Mosafer, J., Hashemi, S.M., Mokhtarzadeh, A., Maleki, A., & Hamblin, M.R. (2020). Recent advances in the application of mesoporous silica-based nanomaterials for bone tissue engineering. Materials Science & Engineering C, Materials for Biological Applications, 107: 110267. https://doi.org/10.1016/j.msec.2019.110267.

[34] Taib, M.N.A.M., Yee, T.S., Trache, D., & Hazwan Hussin, M. (2024). Modification on nanocellulose extracted from kenaf (*Hibiscus cannabinus*) with 3-aminopropyltriethoxysilane for thermal stability in poly (vinyl alcohol) thin film composites. Cellulose, 31(2): 997–1015. https://doi.org/10.1007/s10570-023-05671-1.

[35] Xiang, Z., Guan, X., Ma, Z., Shi, Q., Panteleev, M., & Ataullakhanov, F.I. (2023). Bioactive fibrous scaffolds with programmable release of polypeptides regulate inflammation and extracellular matrix remodeling. Regenerative Biomaterials, 10: rbad010. https://doi.org/10.1093/rb/rbad010.

[36] Liu, X., Hu, Y., Ju, Y., Yang, P., Shen, N., Yang, A., Wu, R., Fang, B., & Liu, L. (2024). Immunomodulatory hydrogels for tissue repair and regeneration. APL Materials, 12(8): 080603. https://doi.org/10.1063/5.0228692.

[37] Yu, R., Zhang, H., & Guo, B. (2021). Conductive Biomaterials as Bioactive Wound Dressing for Wound Healing and Skin Tissue Engineering. Nano-Micro Letters, 14(1): 1. https://doi.org/10.1007/s40820-021-00751-y.

[38] Li, R., Liu, K., & Huang, X. (2022). Bioactive Materials Promote Wound Healing through Modulation of Cell Behaviors. Advanced Science, 9(10): e2105152. https://doi.org/10.1002/advs.202105152.

[39] Aslam Khan, M.U., Aslam, M.A., Bin Abdullah, M.F., & Stojanović, G.M. (2024). Current Perspectives of Protein in Bone Tissue Engineering: Bone Structure, Ideal Scaffolds, Fabrication Techniques, Applications, Scopes, and Future Advances. ACS Applied Bio Materials, 7(8): 5082–5106. https://doi.org/10.1021/acsabm.4c00362.

[40] Ali Abdalla, Y.O., Subramaniam, B., & Nyamathulla, S. (2022). Natural Products for Cancer Therapy: A Review of Their Mechanism of Actions and Toxicity in the Past Decade. Journal of Tropical Medicine, 5794350. https://doi.org/10.1155/2022/5794350.

[41] Shahriar, S.M.S., Andrabi, S.M., Islam, F., & An, J.M. (2022). Next-Generation 3D Scaffolds for Nano-Based Chemotherapeutics Delivery and Cancer Treatment. Pharmaceutics, 14(12). https://doi.org/10.3390/pharmaceutics14122712.

[42] Meng, J., Wang, Z.G., Zhao, X., Wang, Y., Chen, D.Y., Liu, D.L., Ji, C.C., Wang, T.F., Zhang, L.M., Bai, H.X., Li, B.Y., Liu, Y., Wang, L., Yu, W.G., & Yin, Z.T. (2024). Silica nanoparticle design for colorectal cancer treatment: Recent progress and clinical potential. World Journal of Clinical Oncology, 15(6): 667–673. https://doi.org/10.5306/wjco.v15.i6.667.

[43] Xue, R., Pan, Y., Xia, L., & Li, J. (2024). Non-viral vectors combined delivery of siRNA and anti-cancer drugs to reverse tumor multidrug resistance. Biomedicine & Pharmacotherapy, 178: 117119. https://doi.org/10.1016/j.biopha.2024.117119.